

# Doping-induced Polar Defects Improve the Electocaloric Performance of $\text{Ba}_{0.9}\text{Sr}_{0.1}\text{Hf}_{0.1}\text{Ti}_{0.9}\text{O}_3$

Junning Li<sup>1</sup>, Jing Lv,<sup>1</sup> Dawei Zhang,<sup>1</sup> Lixue Zhang,<sup>1</sup> Xihong Hao,<sup>2</sup> Ming Wu,<sup>1</sup> Bai-Xiang Xu,<sup>3</sup> Mojca Otonicar,<sup>4</sup> Turab Lookman,<sup>5</sup> Brahim Dkhil,<sup>6,\*</sup> and Xiaojie Lou<sup>1,†</sup>

<sup>1</sup>Frontier Institute of Science and Technology, and State Key Laboratory for Mechanical Behavior of Materials, Xi'an Jiaotong University, Xi'an 710049, China

<sup>2</sup>Inner Mongolia Key Laboratory of Advanced Ceramic Materials and Devices, Inner Mongolia University of Science and Technology, Baotou 014010, China

<sup>3</sup>Institute of Materials Science, Technical University of Darmstadt, 64287 Darmstadt, Germany

<sup>4</sup>Electronic Ceramics Department, Jožef Stefan Institute, Jamova cesta 39, 1000 Ljubljana, Slovenia

<sup>5</sup>Theoretical Division, Los Alamos National Laboratory, Los Alamos, New Mexico, 87545, USA

<sup>6</sup>Laboratoire Structures, Propriétés et Modélisation des Solides, CentraleSupélec, CNRS-UMR8580, Université Paris-Saclay, 91190 Gif-sur-Yvette, France

(Received 29 September 2020; revised 25 April 2021; accepted 21 June 2021; published 13 July 2021)

In materials science, intentional doping has been widely used to improve the properties of a variety of materials. However, such an approach is not yet exploited in the fast-growing field of electocaloric materials, which represent a serious alternative for next-generation cooling systems. Here we demonstrate with  $\text{Ba}_{0.9}\text{Sr}_{0.1}\text{Hf}_{0.1}\text{Ti}_{0.9}\text{O}_3$ , an ecofriendly ferroelectric material, that doping with 2% of Cu introduces defect dipoles into the ferroelectric matrix and results in (i) enhancement of the adiabatic temperature change  $\Delta T$  by up to 54% while maintaining performance after a large number (up to  $10^4$ ) of electric field cycles, (ii) suppression of the parasitic irreversibility of  $\Delta T$  between *on*-field and *off*-field states, and (iii) an alternative design of refrigeration cycle with a prepoled sample, allowing a two-field-step process showing both conventional ( $\Delta T > 0$ ) and inverse ( $\Delta T < 0$ ) responses when the field is sequentially varied. We also demonstrate that doping significantly increases the energy storage density (by up to 72%). The defect engineering approach therefore offers a path for designing ferroelectrics with improved electocaloric performances. Beyond ferroelectrics, this strategy could also be promising in other solid-state caloric materials (magnetocalorics, elastocalorics, etc.).

DOI: 10.1103/PhysRevApplied.16.014033

## I. INTRODUCTION

During the past decade, electocaloric (EC) materials have been identified as a serious ecofriendly alternative for solid-state refrigeration technologies to replace hazardous gases used in traditional vapor-compression cooling [1,2]. The electocaloric effect (ECE) describes the adiabatic temperature change  $\Delta T$  or isothermal entropy change  $\Delta S$  when an external electric field is applied or withdrawn [3]. In ferroelectric materials, strong EC responses are typically obtained in the vicinity of the Curie temperature  $T_{\text{Curie}}$ , the paraelectric to ferroelectric phase transition [2]. In order to enhance the ECE, great efforts have been put into exploring EC materials and EC concepts and devices [1–12]. Meanwhile, theoretical studies and modeling have been carried out to better understand the physical mechanisms

involved in the ECE and to guide experimentalists [13–16]. Very recently, the influence of different kinds of nonpolar and polar defects on the ECE was studied using molecular dynamics simulations [15]. Such defects enhance the EC temperature span while keeping a large EC response. Further calculations [16,17] have shown that both a conventional (or positive, i.e.,  $\Delta T > 0$  when the electric field  $E \neq 0$ ) and inverse (or negative, i.e.,  $\Delta T < 0$  when  $E \neq 0$ ) ECE could be achieved in  $\text{BaTiO}_3$  ferroelectric samples with antiparallel defect dipoles by tuning the density of defects and the external or internal electric field. Interestingly, defect engineering (e.g., by chemical doping) has already been shown to be an efficient route for tuning ferroelectric and piezoelectric properties [18–22] and thus could also open an avenue for the development of efficient EC materials.

Here, by intentionally introducing defect dipoles into a leadfree  $\text{Ba}_{0.9}\text{Sr}_{0.1}\text{Hf}_{0.1}\text{Ti}_{0.9}\text{O}_3$  (BSHT) ferroelectric material by Cu acceptor doping, we demonstrate experimentally

\*brahim.dkhil@centralesupelec.fr

†x lou03@163.com

that in addition to the significant improvement of the EC response by up to 54% compared with the undoped compound, the ECE shows excellent cycling performance (for up to  $10^4$  cycles) and recovery ability. This ensures a long cycling life, which is a prerequisite for the development of ECE-based devices. Moreover, once the defect-based ferroelectric material is prepoled, an asymmetric polarization state is achieved, allowing a noteworthy response, with both conventional and inverse ECE occurring within a single electric field cycle. We propose that this original cooling cycle is used in upgraded cooling systems, adding to the cooling efficiency. We show that the energy storage density is enhanced by up to 72% thanks to such defect engineering. The use of specific defects is therefore demonstrated to be an efficient strategy for improving the EC response with long-term endurance, which is crucial for refrigeration. Such a defect engineering approach opens a way for the research and design of EC materials with improved performance and cooling concepts, and could be further explored in magnetocaloric or elastocaloric materials, as well as for other applications, such as energy storage capacity for power electronics.

## II. MATERIALS AND METHOD

### A. Sample fabrication and characterization

The  $\text{Ba}_{0.9}\text{Sr}_{0.1}\text{Hf}_{0.1}\text{Ti}_{0.9}\text{O}_3$  (abbreviated as BSHT-0) and 2 mol % CuO-doped  $\text{Ba}_{0.9}\text{Sr}_{0.1}\text{Hf}_{0.1}\text{Ti}_{0.9}\text{O}_3$  (abbreviated as BSHT-2) ceramics are fabricated using a conventional solid-state reaction method with the starting chemicals  $\text{BaCO}_3$  (99.8%),  $\text{SrCO}_3$  (99.99%),  $\text{HfO}_2$  (99.99%),  $\text{TiO}_2$  (99.9%) and  $\text{CuO}$  (99%). Calcination is performed at 1250 °C, and sintering is done at 1365 °C for 4 h in air. The crystalline structure of sintered ceramics is determined by x-ray diffraction (XRD, Shimadzu 7000). The microstructure is observed by a scanning electron microscope (SEM, su-8010). The density of the ceramics is obtained using the Archimedes method. The temperature dependence of the dielectric permittivity is established using a HIOKI 3532 LCR meter. The polarization-electric field (PE) hysteresis loops are recorded using a Radian ferroelectric workstation.

### B. Differential scanning calorimetry equipment

Direct ECE measurements are carried out with a modified differential scanning calorimeter (DSC, TA Instruments Q2000). Additionally, the frequencies of switching the applied field on and off are of the same magnitude (around  $200 \text{ V s}^{-1}$ ) in order to eliminate the dependence of the ECE on field frequency. At each temperature point, we perform three measurements with the electric field both on and off. Thus, we have six values of  $\Delta T$  calculated for each experimental point (three with the field on and three with the field off). The mean values and standard deviation

(error bars) are then estimated [23]. The calibration of thermal loss in our DSC is based on Ref. [24]. The thermal loss correction factor  $K$  shows a second-order polynomial dependence on temperature, which is considered in our data analysis. Considering errors from equipment and the data analysis process, the error in our experimental data is  $\pm 10\%$ .

## III. CONSEQUENCES OF DIPOLAR DEFECTS ON HYSTERESIS LOOP AND ENERGY STORAGE

Figure 1(a) depicts a phase diagram of the leadfree  $x\text{Ba}_{0.8}\text{Sr}_{0.2}\text{TiO}_3-(1-x)\text{BaHf}_{0.2}\text{Ti}_{0.8}\text{O}_3$  (BSHT) solid solution system, which is established based on the temperature-dependent dielectric permittivity and XRD data of the BSHT ceramics, fabricated by a conventional solid-state reaction route [25]. Since the proximity of phases with different symmetries is believed to produce a large ECE [6], we study the critical point composition where several phases coexist in the phase diagram, located at  $x = 0.5$  and  $T = 56^\circ\text{C}$ , i.e., the BSHT-0 sample.  $\text{Cu}^{2+}$  defects as acceptor dopants are introduced during the ceramic fabrication (see Materials and method section) through the addition of 2 mol %  $\text{CuO}$  to  $\text{Ba}_{0.9}\text{Sr}_{0.1}\text{Hf}_{0.1}\text{Ti}_{0.9}\text{O}_3$  (to make BSHT-2). Figure 1(b) shows the temperature dependence of the dielectric permittivity at 100 Hz upon cooling the BSHT-0 and BSHT-2 ceramics. The maximum of the dielectric constant  $\varepsilon_{\max}$ , which is related to the paraelectric to ferroelectric phase transition, occurs at  $T_{\text{Curie}} = 56^\circ\text{C}$  in BSHT-0, while it is reduced by approximately 3 °C for the doped BSHT-2 sample. Its magnitude increases by approximately 24%, going from  $\varepsilon_{\max} = 13\,775$  for BSHT-0 to  $\varepsilon_{\max} = 17\,029$  in the case of BSHT-2. Moreover, doping causes broadening of the dielectric peak, which can further be associated with the temperature dependence of the specific heat capacity, presented in Fig. 1(c). Indeed, the exothermic peak is smoothed in the doped case, showing that the phase transition becomes more diffuse with doping. The room-temperature PE loops of the BSHT-0 and BSHT-2 samples are plotted in Figs. 1(d)–1(f) for a maximum applied field of  $10 \text{ kV cm}^{-1}$ . The BSHT-0 sample shows a typical hysteresis loop for a normal ferroelectric state with remanent ( $P_r$ ) and maximum polarization ( $P_{\max}$ ) at  $10 \text{ kV cm}^{-1}$  of  $5.14$  and  $11.73 \mu\text{C cm}^{-2}$ , respectively. In contrast, the Cu-doped BSHT-2 sample displays a “pinched” PE loop that is characteristic of the presence of defect dipoles [26,27]. Indeed, the introduction of the  $\text{Cu}^{2+}$  acceptor dopant by replacing  $\text{Ti}^{4+}/\text{Hf}^{4+}$  brings an effective negative charge that is compensated for by the oxygen vacancies [19,28] (intrinsic ones and those arising from the  $\text{CuO}$  doping). Following the  $\text{Cu}^{2+} \xrightarrow{\text{Ti}^{4+}/\text{Hf}^{4+}} \text{Cu}''_{\text{Ti/Hf}} + \text{V}_\text{O}^-$  process,  $\text{Cu}_{\text{Ti/Hf}}^{2-} - \text{V}_\text{O}^{2+}$  defect dipoles are created. As they are randomly distributed in the ferroelectric phase, they act as local and static random fields, causing the switchable and free moving ferroelectric dipoles to be

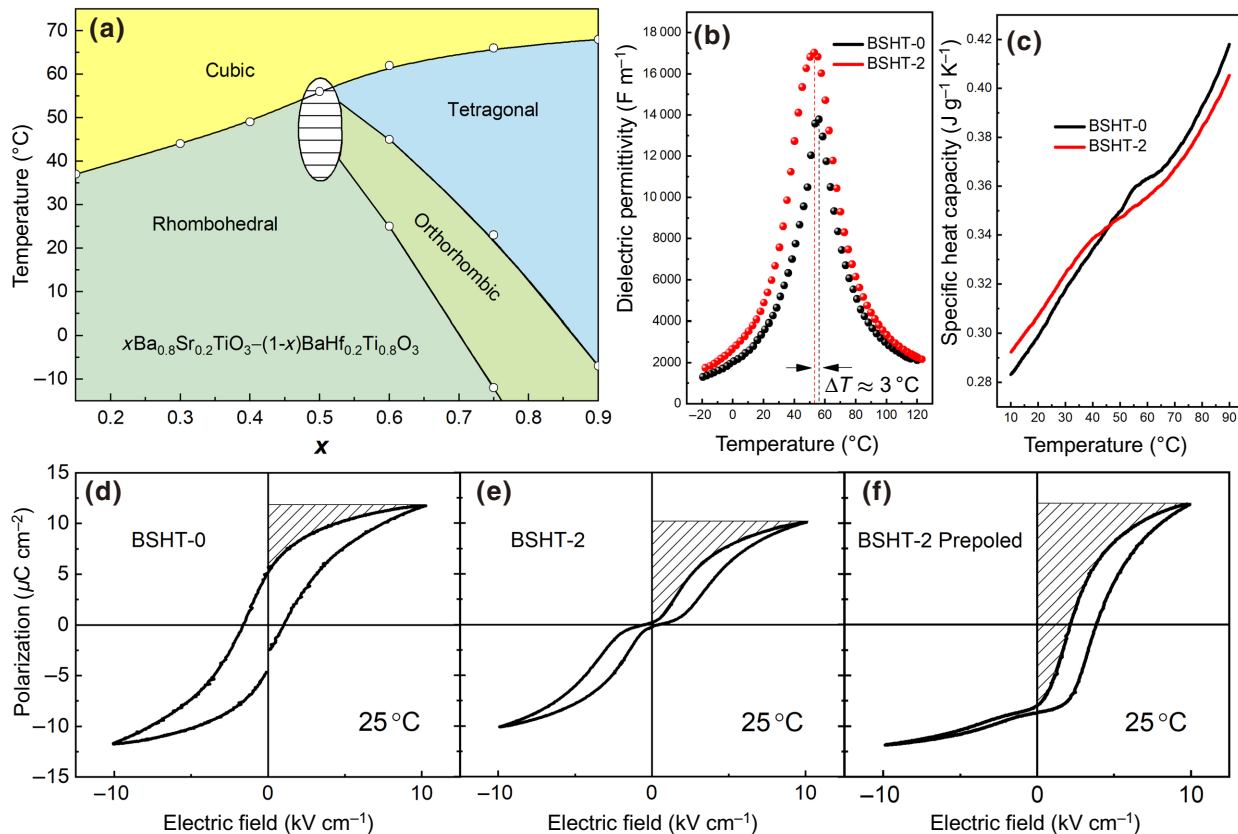


FIG. 1.  $\text{Ba}_{0.8}\text{Sr}_{0.2}\text{TiO}_3$ – $\text{BaHf}_{0.2}\text{Ti}_{0.8}\text{O}_3$  (BSHT) phase diagram and dielectric and polarization behavior without and with intentional Cu doping. (a) The phase diagram of the BSHT system constructed using the dielectric permittivity versus temperature results. (b) and (c) Temperature dependence of dielectric permittivity (at 100 Hz; cooling rate, 3 °C/min) and specific heat capacity of BSHT-0 and BSHT-2 samples. Room-temperature  $PE$  loops (at 10 Hz). (d) The normal  $PE$  loop of BSHT-0. (e) The appearance of the pinched hysteresis loop for BSHT-2. (f) The shifted single hysteresis loop for prepoled BSHT-2.

locally aligned with those fields. In the end, the random distribution of all the dipoles gives rise to a zero net polarization in the absence of an external field, while application of a field surpasses the local fields and triggers the mobile dipoles. This gives rise to the pinched  $PE$  loop in Fig. 1(e) where  $P_{\max}$  of the Cu-doped BSHT-2 sample reaches  $10.10 \mu\text{C cm}^{-2}$  at  $10 \text{ kV cm}^{-1}$ , and then drops down to almost zero ( $P_r = 0.14 \mu\text{C cm}^{-2}$ ) when the electric field is switched off. It is worth noting the reduction in  $P_{\max}$  of approximately 14% compared with that of the hysteresis loop, i.e., both  $P_{\max}$  and  $P_r$  can thus be controlled by tuning the concentration and the nature of defect dipoles to reach optimal conditions for the ECE, as, for instance, polar materials with a large  $P_{\max}$  and concomitantly small  $P_r$  should exhibit a larger entropy change. In order to align the static defect dipoles along the same direction, the BSHT-2 sample is prepoled at  $120$  °C (above  $T_{\text{Curie}}$ ) under a saturating dc bias of  $20 \text{ kV cm}^{-1}$  for 1 h, and field cooled. As seen in Fig. 1(f), the prepoled BSHT-2 specimen exhibits a completely different  $PE$  loop compared with the unpoled one [see Fig. 1(d)], that is, a “shifted” single loop into the positive-field-value region, resulting in a negative  $P_r$ ,

at zero field. This is explained by the effect of the internal field ( $E_d$ ) induced by the alignment of the defect dipoles (or static local fields) and this  $E_d$  bias can be determined as [20,26]

$$E_d = (E_c^+ + E_c^-)/2 \quad (1)$$

where  $E_c^+$  and  $E_c^-$  are the relative coercive fields (at  $P=0$ ) when a high positive and low positive electric field is applied, respectively.  $E_d$  and  $E_c$ , the coercive field, ( $2E_c = |E_c^+| - |E_c^-|$ ), estimated from the  $PE$  curve at  $10 \text{ kV cm}^{-1}$ , are  $3.02$  and  $0.85 \text{ kV cm}^{-1}$ , respectively.  $PE$  curves measured at various electric fields up to  $50 \text{ kV cm}^{-1}$  for the prepoled BSHT-2 sample (see Fig. S4 of the supplemental material [25]) show that  $E_d$  is always larger than  $E_c$  meaning that the intentionally introduced defect dipoles are therefore expected to strongly stabilize the polarization to either an up or down state, depending on the direction of the poling field preliminarily applied; here [Fig. 1(f)] the downward macroscopic polarization is favored.

By designing the polarization state and therefore the shape of the  $PE$  curve in ferroelectrics, there is an

TABLE I. The energy storage properties for BSHT-0, BSHT-2 and prepoled BSHT-2 samples under  $50 \text{ kV cm}^{-1}$ .

Samples	Energy storage ( $\text{J cm}^{-3}$ )	Energy efficiency (%)
BSHT-0	0.11	47.83
BSHT-0 aging	0.11	47.83
BSHT-2	0.18	85.71
BSHT-2 aging	0.20	86.32
Poled BSHT-2	0.17	73.91
Poled BSHT-2 aging	0.21	78.91

immediate consequence of this defect engineering on the energy storage density  $J_{\text{stor}}$ , which corresponds to the area between the polarization axis and the discharging curve (i.e., the upper branch) of the  $PE$  curve [see dashed region in Figs. 1(d)–1(f)]. The larger such an area is, the higher the energy stored by the capacitor. The losses,  $J_{\text{loss}}$ , are also minimized by decreasing the area between the discharge (upper branch) and charge (lower branch) curves in order to enhance the energy storage efficiency  $\eta = [J_{\text{stor}}/(J_{\text{stor}} + J_{\text{loss}})] \times 100\%$ . Table I shows that the energy storage density  $J_{\text{stor}}$  and its efficiency  $\eta$  when doping is significantly enhanced for Cu-doped BSHT-2 compared with the undoped sample BSHT-0 by up to approximately 64% and 79%, respectively, with a maximum applied field of  $E_{\text{max}} = 50 \text{ kV cm}^{-1}$ . When the doped sample is prepoled (i.e., BSHT-2), there is also an improvement in the storage ability performance;  $J_{\text{stor}} = 0.17 \text{ J cm}^{-3}$  at  $50 \text{ kV cm}^{-1}$ , which is comparable with the energy density reported for bulk ferroelectric ceramics [e.g.,  $J_{\text{stor}} = 0.37 \text{ J cm}^{-3}$  at  $90 \text{ kV cm}^{-1}$  in bulk BST (BST refers to  $\text{Ba}_{0.4}\text{Sr}_{0.6}\text{TiO}_3$ ) [29] or  $J_{\text{stor}} = 0.57 \text{ J cm}^{-3}$  at  $56 \text{ kV cm}^{-1}$  in bulk  $0.89\text{BNT-0.06BT-0.05KNN}$  (BNT refers to  $\text{Bi}_{0.5}\text{Na}_{0.5}\text{TiO}_3$ ; BT refers to  $\text{BaTiO}_3$ ; KNN refers to  $\text{K}_{0.5}\text{Na}_{0.5}\text{NbO}_3$ ) [30]]. Note that the energy storage density is typically less than  $1 \text{ J cm}^{-3}$  because of the low dielectric breakdown strength (typically lower than  $100 \text{ kV cm}^{-1}$ ). Nonetheless, it could be significantly increased by improving the dielectric capacitor properties through grain size optimization, composite formation (using a glass additive, for instance) or in a thin-film form [31]. Therefore, appropriate doping as done here by inducing defect dipoles could also be a strategy for designing ferroelectrics with enhanced energy storage capabilities.

#### IV. DEFECT ENGINEERING OF ELECTROCALORIC RESPONSE

Let us now investigate the effect of doping on the electrocaloric properties. To evaluate the specific heat exchange values ( $\Delta Q$ ), the area under the exothermic and endothermic peaks is integrated. Then, the isothermal EC temperature change ( $\Delta T$ ) is estimated according to the

following equation [19]:

$$\Delta T = \frac{\Delta Q}{c_p} K \quad (2)$$

where  $c_p$  is the specific heat capacity and  $K$  is the thermal loss factor [32]. Any contribution related to Joule heating can be neglected or corrected from the DSC signal, which should return to the baseline after the field is switched *off* [25]. The determined  $\Delta T$  values at different electric fields for BSHT-0 and BSHT-2 ceramics at room temperature when the electric field is *on* are depicted in Fig. 2(a). For BSHT-0,  $\Delta T$  is about  $0.04 \pm 0.004 \text{ K}$  under  $10 \text{ kV cm}^{-1}$  and reaches  $0.19 \pm 0.019 \text{ K}$  under  $20 \text{ kV cm}^{-1}$ . Above  $20 \text{ kV cm}^{-1}$ , the BSHT-0 ceramic unfortunately experiences a breakdown and therefore no EC data can be recorded. In contrast, for BSHT-2, it is still possible to apply a field at least as high as  $30 \text{ kV cm}^{-1}$  up to  $65^\circ\text{C}$ , reaching a  $\Delta T = 0.37 \pm 0.037 \text{ K}$  at room temperature, and showing that the doping is beneficial for achieving a higher breakdown resistance. In fact,  $\Delta T$  increases significantly in the doped BSHT-2 compared to the undoped BSHT-0; the doped sample attains  $0.07 \pm 0.007 \text{ K}$  under  $10 \text{ kV cm}^{-1}$  and  $0.23 \pm 0.023 \text{ K}$  under  $20 \text{ kV cm}^{-1}$ , which corresponds to an average increase of 54% and 26% with respect to the undoped sample, respectively. Note also that while  $\Delta T$  at room temperature is rather weak (because the critical temperature is far from room temperature), the electrocaloric strength (i.e.,  $\Delta T/E$ ) remains comparable with that of general electrocaloric materials [25]. Figures 2(b) and 2(c) show the temperature dependence of  $\Delta T$  extracted from the direct heat flow curves under a field of  $10 \text{ kV cm}^{-1}$  [25]. In Fig. 2(b), the  $\Delta T$  values of BSHT-0 reach a maximum around the Curie temperature, as expected, and  $\Delta T$  is equal to  $0.20 \pm 0.02 \text{ K}$  at  $65^\circ\text{C}$  under  $10 \text{ kV cm}^{-1}$ . It is worth noting that there is an asymmetry (irreversibility) in the caloric response when the electric field is applied (*on* state) and withdrawn (*off* state), which is better evidenced below  $T_{\text{Curie}}$  [Fig. 2(b)]. For example, the  $\Delta T$  value of the *off* state is  $0.04 \text{ K}$  at  $25^\circ\text{C}$  [see Fig. 2(b) and inset], while it is  $0.09 \text{ K}$  in the *on* state, i.e., twice as big. This large  $\Delta T$  gap between the field being *on* and *off* due to the ferroelectric state is always considered to be detrimental for EC performance [6,33,34]. Note that this asymmetry exists even when cycling the electric field and the full mechanism of its origin remains to be understood. In contrast, for the doped BSHT-2 sample, the exothermic and endothermic peaks are of the same magnitude in continuously repeated cycles [25]. For instance, under  $10 \text{ kV cm}^{-1}$ ,  $\Delta T$  values for both the *on* and the *off* state are the same, about  $0.22 \text{ K}$  at  $55^\circ\text{C}$ , and around  $0.07 \text{ K}$  at  $25^\circ\text{C}$ . Figure 2(d) schematically presents the refrigeration cycle in the  $T$ - $E$  diagram, comparing responses of both BSHT-0 and BSHT-2. The diagram nicely shows the asymmetry between the *on* and *off* states in BSHT-0, with initial temperature retrieved

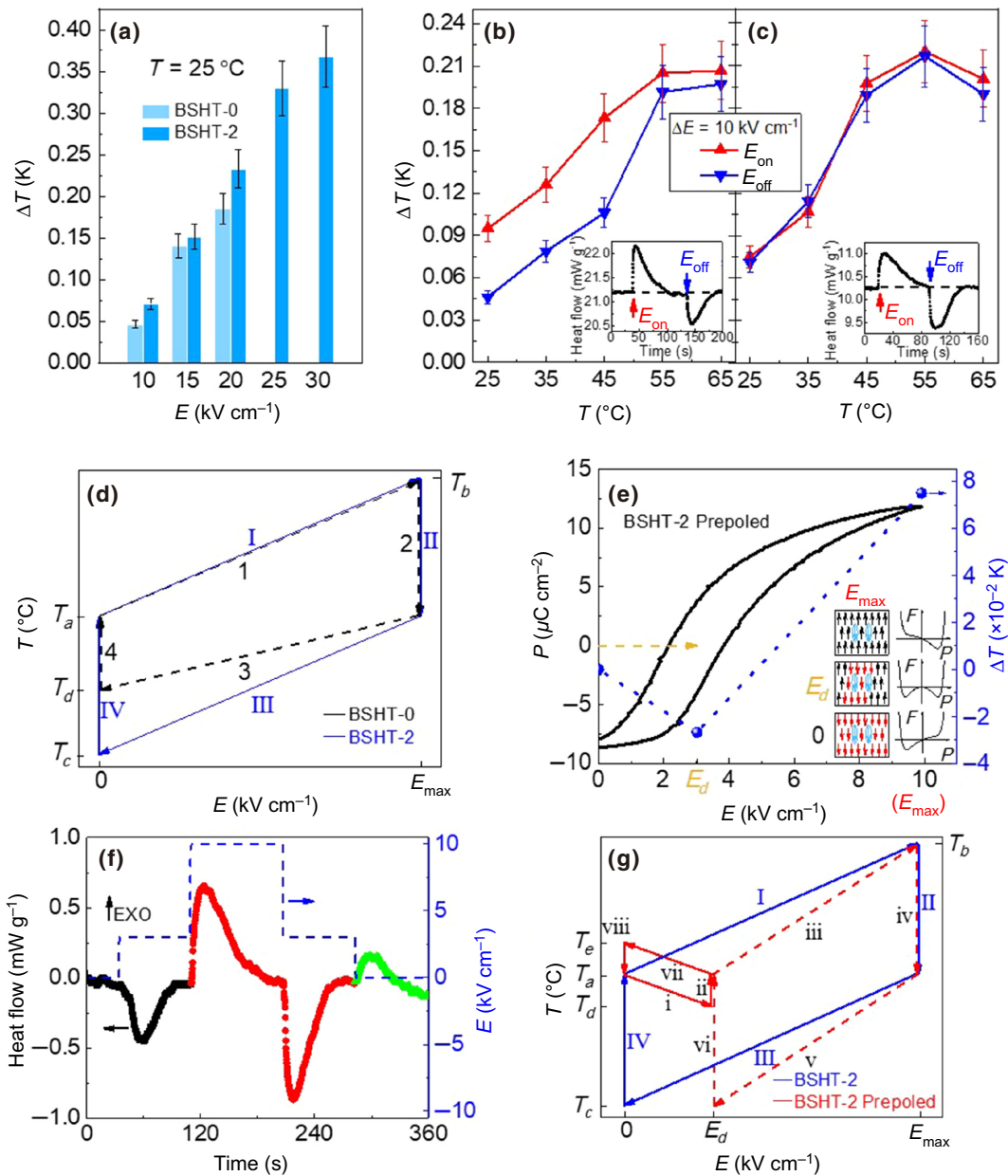


FIG. 2. Electocaloric response and defect dipole consequences. (a) The direct temperature change ( $\Delta T$ ) in the field *off* regime for BSHT-0 and BSHT-2 samples measured under different electric fields at room temperature. (b) and (c) Directly measured values of  $\Delta T$ , as a function of temperature, under the application ( $E_{on}$ ) and removal ( $E_{off}$ ) of the electric field ( $10 \text{ kV cm}^{-1}$ ). The insets show the directly recorded heat flow signal as the electric field is turned on and off. Dashed line is drawn to show the isothermal process. (d) Two idealized refrigeration cycles proposed for BSHT-0 and BSHT-2. (e) The  $P$ - $E$  loop and direct  $|\Delta T|$  values of poled BSHT-2. The insets show the schematic configurations in a single domain pattern with defect dipoles and the connection between the Landau free energy ( $F$ ) and polarization ( $P$ ) under external electric field in prepoled BSHT-2. (f) The signal of direct ECE measurements for poled BSHT-2. (g) An idealized refrigeration cycle that utilizes both negative and positive ECE (steps i–viii) based on a prepoled BSHT-2 sample compared with the conventional cycle (steps I–IV). The cycle begins (step i) with the adiabatic application of a low electric field ( $E_d$ ) that causes cooling of the material via the negative ECE ( $\Delta T_n = |T_a - T_d|$ ). Then, the cold body absorbs heat from the environment under constant  $E_d$  (step ii) and the system returns to  $T_a$ . In step iii, the adiabatic application of a large electric field ( $\Delta E = E_M - E_d$ ) results in an increase in the temperature of the material. The material then returns to the original  $T_a$  by heat exchange with a sink under constant  $E_M$  (step iv). In step v,  $E_M$  decreases adiabatically to  $E_d$ , leading to a drop in the temperature to  $T_c$  via a positive ECE ( $\Delta T_p = |T_a - T_c|$ ). In step vi the system returns to the original  $T_a$  by absorbing heat from the load. The cycle closes via adiabatic removal (decrease) of  $E_d$  (step vii) followed by heat exchange with a sink (step viii). Overall, the final temperature change is enhanced to  $\Delta T = \Delta T_n + \Delta T_p$ . Note: All the temperature terms in (d) and (g) are used for better illustration; they are not actual values. Specifically,  $T_a$  is the initial temperature of the sample and  $T_b$ ,  $T_c$ ,  $T_d$ , and  $T_e$  are the corresponding temperatures induced by the ECE.

by another path with field *off* as compared with field *on* (branch 1 is not parallel to branch 3, while in case of BSHT-2 branches I and III are parallel). This effect is also observed from the *PE* loops where the polarization *P* has a different value at  $E=0$  for BSHT-0 to that in the case of BSHT-2, where the latter shows a pinched curve. Thus, in addition to the significant improvement of  $\Delta T$  magnitudes, doping with the goal of achieving defect dipoles is also very beneficial for caloric cycling owing to the suppression of the asymmetry between the field *on* and *off* states.

Let us now consider the shifted single loop obtained by poling BSHT-2, as it can provide a design approach for cooling. Figure 2(e) shows, in addition to the positively shifted single *PE* loop, the directly measured  $\Delta T$  at room temperature for the prepoled BSHT-2 when the electric field is increased from 0 to  $E_d = 3 \text{ kV cm}^{-1}$  and then to  $E_{\max} = E_M = 10 \text{ kV cm}^{-1}$  [Fig. 2(f)]. Interestingly, as shown in Figs. 2(e) and 2(f), a negative temperature change (endothermic) of  $|\Delta T| = 0.03 \text{ K}$  by inverse ECE is observed when the field is turned *on* (0 to  $E_d$ ). The inverse ECE has been explained in a simple manner in antiferroelectrics [35] where the antiferroelectric state, i.e., the antipolar dipole arrangement, is destabilized by application of the external field resulting in an increase of the disorder (entropy) and thus  $\Delta T$  becomes negative. Here, with the doped sample, the situation is similar to that of antiferroelectrics as the electric field has to disorder the polar order imposed with the defect dipoles and this increase in the entropy gives rise to a negative  $\Delta T$ . Then, in a second stage when a larger field is applied ( $E_d$  to  $E_M$ ), the temperature rises, leading to  $\Delta T = 0.07 \text{ K}$  through a conventional (exothermic) or positive ECE. Note that this latter value obtained at  $10 \text{ kV cm}^{-1}$  is comparable with the one obtained for the unpoled doped BSHT-2 sample [Fig. 2(c)]. Poling does not seem to improve the  $\Delta T$  amplitude at maximum electric field. When the electric field is switched off, the system comes back to its initial state through the positive and the negative effect, i.e., with an endothermic heat flux signal followed by an exothermic one when the  $E_d$  field is reached [Fig. 2(f)]. Having within the same electric field cycle both the inverse and conventional caloric effects, achievable by sequentially tuning the applied electric field amplitude is remarkable and thus can be considered as a refrigeration cycle. However, it should be clarified that if one immediately applies the electric field from zero to the maximum value and does not pass sequentially through stops at intermediate field values, then the inverse effect cannot be detected. This refrigeration cycle is schematically presented in Fig. 2(g), in comparison with the “classical” cycle observed for the unpoled BSHT-2 sample. In this cooling cycle, one can use a two-field step (without field reversal [36]), one of small amplitude (below  $E_d$ ) to achieve a negative EC cycle ( $\Delta T_n = |T_a - T_d|$ ) followed by a higher field strength (above  $E_d$ ) to

obtain a positive EC cycle ( $\Delta T_p = |T_a - T_c|$ ). In the end (at  $E=0$ ), the final temperature change is enhanced to  $\Delta T = \Delta T_n + \Delta T_p$ . Therefore, this defect engineering approach allows us to demonstrate experimentally an alternative two-field-step cycle, opening perspectives for refrigeration concepts beyond electrocalorics.

## V. CYCLING STABILITY AND REJUVENATION

In order to ensure the suitability of the doped samples for refrigeration, the cycling stability of the EC response under different electric fields and high cycling frequencies needs to be studied. For this purpose, the two doped samples (BSHT-2 and prepoled BSHT-2) are cycled at room temperature (i.e., within the ferroelectric phase) with a bipolar electric field signal at 10 Hz with different electric fields, i.e., 10 and  $30 \text{ kV cm}^{-1}$  (see Figs. 3 and Ref. [25]) for up to  $10^4$  bipolar cycles (one bipolar cycle includes two EC cooling cycles). Unipolar fatigue measurements are also performed but unfortunately the polarization and  $\Delta T$  degrade quickly. For unpoled BSHT-2 [Figs. 3(a)–3(c)] under  $30 \text{ kV cm}^{-1}$ , the  $P_{\max}$  value rises from  $14.4 \mu\text{C cm}^{-2}$  to  $16.3 \mu\text{C cm}^{-2}$  after  $10^4$  cycles, which is an increase of 13.2% while the coercive field  $E_c$  remains almost unchanged. Concomitantly to the increase of  $P_{\max}$  with cycling,  $P_r$  of BSHT-2 rises by about 340% with  $E_{\max} = 30 \text{ kV cm}^{-1}$  (240% with  $E_{\max} = 10 \text{ kV cm}^{-1}$ ) and thus the pinched loop forms a more ferroelectriclike one after  $10^4$  cycles [25]. A similar increase in the remanence with cycling was also observed recently in  $\text{Pb}(\text{Ti}, \text{Zr})\text{O}_3$  ceramics [37]. It is worth noting that the achieved value of  $+P_r$  ( $1.50 \mu\text{C cm}^{-2}$  at  $10 \text{ kV cm}^{-1}$ ) after  $10^4$  cycles remains much lower than the one in normal ferroelectric BSHT-0 ( $5.14 \mu\text{C cm}^{-2}$  at  $10 \text{ kV cm}^{-1}$ ; see Ref. [25]). We believe this phenomenon corresponds to the training process of the defect dipoles, which begin to respond after a large number of electric field cycles [38]. Interestingly, we find that all the *PE* loop data (i.e.,  $P_{\max}$ ,  $P_r$ , and  $E_c$ ) return back to the original state when the cycling of the electric field is stopped and the sample is kept at room temperature for 24 h (Fig. 3 and Ref. [25]). This phenomenon corresponds to the aging effect, which depends on the time and the temperature at which it is realized [20,26].

For the prepoled BSHT-2 sample [Figs. 3(e)–3(g) and Ref. [25]], after  $10^4$  cycles,  $P_{\max}$  at  $30 \text{ kV cm}^{-1}$  shows only slight changes as it increases by 4.5% reaching a value of  $16.2 \mu\text{C cm}^{-2}$ ;  $P_r$  demonstrates the same trend. After 24 h aging,  $P_{\max}$  remains unchanged and does not show any reduction, while  $P_r$  slightly reduces from  $-10.8 \mu\text{C cm}^{-2}$  to  $-11.3 \mu\text{C cm}^{-2}$ , corresponding to a variation of 4.6%. Interestingly, the positively shifted *PE* loop of the prepoled BSHT-2 sample remains shifted after  $10^4$  cycles [25], with the coercive field  $E_c$  only weakly varying, if at all, while the internal bias field  $E_d$  decreases by about 25% to reach  $2.4 \text{ kV cm}^{-1}$  [Fig. 3(g)]. Nonetheless,  $E_d$  and  $E_c$  return to

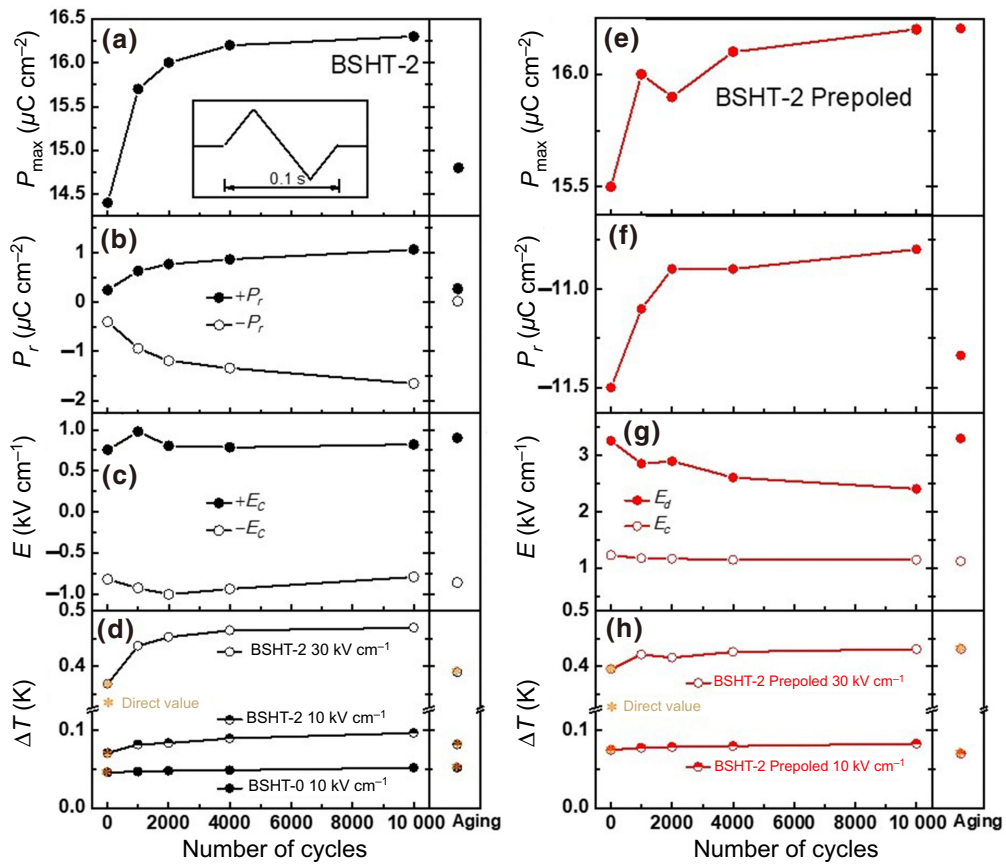


FIG. 3. Electrocaloric response after cycling and aging. The durability test to confirm the cycling and cooling stability of the BSHT-2 and poled BSHT-2 samples under  $30 \text{ kV cm}^{-1}$ . (a)–(c)  $P_{\max}$ ,  $P_r$ , and  $E_c$  of BSHT-2 as a function of the number of cycles under  $30 \text{ kV cm}^{-1}$ . (d) The direct and indirect  $\Delta T$  changes for BSHT-0 and BSHT-2 samples as a function of the number of cycles for 10 and  $30 \text{ kV cm}^{-1}$ , respectively. (e)–(g) The  $P_{\max}$ ,  $P_r$ ,  $E_c$ , and  $E_d$  for prepoled BSHT-2 as a function of the number of cycles under  $30 \text{ kV cm}^{-1}$ . (h) The direct and indirect  $\Delta T$  change for prepoled BSHT-2 samples as a function of the number of cycles for 10 and  $30 \text{ kV cm}^{-1}$ , respectively. The data in the right hand area is from cycled samples after aging for 24 h. The waveform of the electric field for fatigue testing is shown in the inset.

their initial state after the cycling electric field is removed and aging for 24 h at room temperature. Therefore, the prepoled BSHT-2 sample keeps its shifted PE loop characteristics after up to  $10^4$  cycles. This cycling stability shows potential for the use of the refrigeration cycle based on the two-field-step approach [Figs. 2(f) and 2(g)] for future cooling devices. Moreover, an aging step can also be added into the process in order to rejuvenate the sample and thus to further improve the cycling life of the refrigeration device.

Considering the isothermal conditions imposed during the direct measurement process, the direct temperature change ( $\Delta T$ ) cannot be recorded in a reasonable time during the cycling process. Thus, in order to quantify the ECE during the cycling process, we use the indirect approach using the Landau free energy,  $F$ , which can be expanded in terms of polarization ( $P$ ) according to

$$F = \frac{1}{2}\alpha P^2 + \frac{1}{2}\gamma P^4 + \frac{1}{2}\delta P^6 - EP \quad (3)$$

where  $\alpha = \beta(T - T_{\text{Curie}})$  with  $\beta$  being the Curie constant, the coefficients  $\gamma$  and  $\delta$  are assumed to be temperature independent, and the electric field  $E$  is the sum of the external field  $E_{\text{ext}}$  and the internal field arising from dipole defects  $E_d$ . The dipolar entropy  $S$  can be expressed as  $-(\partial G/\partial T)_P = -\beta P^2/2$ . Therefore, the entropy change  $\Delta S$ , from its initial state with polarization  $P_0$  to another state with polarization  $P$  can be expressed as  $\Delta S = -\beta TP^2/2 + \beta T_0 P_0^2/2$  and the adiabatic temperature change is  $\Delta T = \beta TP^2/2c_p$ , where  $c_p$  is the specific heat capacity [39]. Thus, one sees that  $\Delta T$  is related to the values of  $\beta$  and the polarization ( $P$ ). In working conditions with a given temperature and electric field, we consider the value of  $c_p$  and  $\beta$  to be constant. Therefore, before cycling, we use direct  $\Delta T$  data (for BSHT-2, direct  $\Delta T$  is about  $0.368^\circ\text{C}$  under  $30 \text{ kV cm}^{-1}$  at room temperature) to determine the value of  $\beta$  that we use to determine  $\Delta T$  from the polarization during the cycling process. Figure 3(d) shows the indirect  $\Delta T$  change in the doped BSHT-2 sample for up to  $10^4$  cycles. For an electric field of  $30 \text{ kV cm}^{-1}$ , BSHT-2

has a  $\Delta T$  that rises from 0.37 to 0.44 K after  $10^3$  cycles and reaches 0.47 K after  $10^4$  cycles, meaning that in the end  $\Delta T$  increases by more than 27.7%. By cycling with a field of  $10 \text{ kV cm}^{-1}$ , the  $\Delta T$  of BSHT-2 also increases by up to 36.6%, from 0.07 K to 0.1 K after  $10^4$  cycles. As the undoped BSHT-0 could not sustain  $30 \text{ kV cm}^{-1}$ , we compare it for a field of  $10 \text{ kV cm}^{-1}$ , where we see no change in  $\Delta T$ , as it remains at approximately 0.05 K. It is interesting to note that even after a large number of cycles the material is still able to provide an EC temperature change and that the Cu-dopant significantly increases the  $\Delta T$  value, which continues to increase with cycling, in contrast to the undoped sample. Finally, the aging process allows  $\Delta T$  to recover its initial value. Figure 3(h) depicts the evolution of the indirect  $\Delta T$  values of prepoled BSHT-2 during the cycling process. As with the unpoled BSHT-2 sample [Fig. 3(d)], the  $\Delta T$  of the prepoled BSHT-2 sample [Fig. 3(h)] increases from 0.4 to 0.43 K after  $10^4$  cycles, corresponding to an enhancement of 7.5%, meaning that such an engineered (doped and prepoled) sample can be useful for a large number of cycles and efficient electrocaloric responses.

## VI. CONCLUSION

In summary, we show that doping by introducing defect dipoles into ferroelectrics, such as BSHT ceramics, can be used as an elegant approach to tailor electrocaloric materials. It is a way to provide a more efficient electrocaloric response, which maintains or can rejuvenate its performance after a large number of cycles and can be used in an alternative refrigeration cycle through a two-field step. We believe that such approach can be further explored in various ferroelectrics [40,41] and also in other solid-state calorics, such as magnetocalorics or elastocalorics. Moreover, beyond the caloric properties, such a materials design approach can also be exploited for energy storage purposes.

## ACKNOWLEDGMENTS

This work is supported by the National Science Foundation of China (NSFC No. 51372195 and No. 51772238), the CSS project (Grant No. YK2015-0602006), the Fundamental Research Funds for the Central Universities and the World-Class Universities (Disciplines), and the Characteristic Development Guidance Funds for the Central Universities. J.L. would like to thank J. F. Scott, P. Lloveras, V. Shvartsman, D. Xue, and Y. T. Wang for their fruitful discussions and help. X.L. would like to thank the “One Thousand Youth Talents” program for support. Support from National Key R&D Program of China (2017YFA0208000) is also appreciated. B.D. and M.O. acknowledge a public grant overseen by the French National Research Agency (ANR) as part of the “Investissements d’Avenir” program

(Reference No. ANR-10-LABX-0035, LabexNanoSaclay) and PHC Slovenian-French Proteus project BI-FR/19-20-PROTEUS-009.

- 
- [1] S. P. Alpay, J. Mantese, S. Trolier-McKinstry, Q. Zhang, and R. W. Whatmore, Next-generation electrocaloric and pyroelectric materials for solid-state electrothermal energy interconversion, *MRS Bull.* **39**, 1099 (2014).
  - [2] X. Moya, X. Moya, S. Kar-Narayan, and N. D. Mathur, Caloric materials near ferroic phase transitions, *Nat. Mater.* **13**, 439 (2014).
  - [3] J. Scott, Electrocaloric materials, *Annu. Rev. Mater. Res.* **41**, 229 (2011).
  - [4] A. S. Mischenko, Q. Zhang, J. F. Scott, R. W. Whatmore, and N. D. Mathur, Giant electrocaloric effect in thin-film  $\text{PbZr}_{0.95}\text{Ti}_{0.05}\text{O}_3$ , *Science* **311**, 1270 (2006).
  - [5] F. Le Gouplil, J. Bennett, A.-K. Axelsson, M. Valant, A. Berenov, A. J. Bell, T. P. Comyn, and N. M. Alford, Electrocaloric enhancement near the morphotropic phase boundary in lead-free NBT-KBT ceramics, *Appl. Phys. Lett.* **107**, 172903 (2015).
  - [6] J. Li, D. Zhang, S. Qin, T. Li, M. Wu, D. Wang, Y. Bai, and X. Lou, Large room-temperature electrocaloric effect in lead-free  $\text{BaHf}_x\text{Ti}_{1-x}\text{O}_3$  ceramics under low electric field, *Acta Mater.* **115**, 58 (2016).
  - [7] Q. Li, G. Zhang, X. Zhang, S. Jiang, Y. Zeng, and Q. Wang, Relaxor ferroelectric-based electrocaloric polymer nanocomposites with a broad operating temperature range and high cooling energy, *Adv. Mater.* **27**, 2236 (2015).
  - [8] A. Grünebohm, M. Marathe, and C. Ederer, Tuning the caloric response of  $\text{BaTiO}_3$  by tensile epitaxial strain, *Europhys. Lett.* **115**, 47002 (2016).
  - [9] Y. Liu, I. C. Infante, X. Lou, D. C. Lupascu, and B. Dkhil, Giant mechanically-mediated electrocaloric effect in ultra-thin ferroelectric capacitors at room temperature, *Appl. Phys. Lett.* **104**, 012907 (2014).
  - [10] A. Chauhan, S. Patel, and R. Vaish, Multicaloric effect in  $\text{Pb}(\text{Mn}_{1/3}\text{Nb}_{2/3})\text{O}_3\text{-}32\text{PbTiO}_3$  single crystals, *Acta Mater.* **89**, 384 (2015).
  - [11] X. S. Qian, H. J. Ye, Y. T. Zhang, H. Gu, X. Li, C. Randall, and Q. Zhang, Giant electrocaloric response over a broad temperature range in modified  $\text{BaTiO}_3$  ceramics, *Adv. Funct. Mater.* **24**, 1300 (2014).
  - [12] J. Koruza, B. Rožič, G. Cordoyiannis, B. Malič, and Z. Kutnjak, Large electrocaloric effect in lead-free  $\text{K}_{0.5}\text{Na}_{0.5}\text{NbO}_3\text{-SrTiO}_3$  ceramics, *Appl. Phys. Lett.* **106**, 202905 (2015).
  - [13] I. Ponomareva and S. Lisenkov, Bridging the Macroscopic and Atomistic Descriptions of the Electrocaloric Effect, *Phys. Rev. Lett.* **108**, 167604 (2012).
  - [14] M. C. Rose and R. E. Cohen, Giant Electrocaloric Effect Around  $T_c$ , *Phys. Rev. Lett.* **109**, 187604 (2012).
  - [15] A. Grünebohm and T. Nishimatsu, Influence of defects on ferroelectric and electrocaloric properties of  $\text{BaTiO}_3$ , *Phys. Rev. B* **93**, 134101 (2016).
  - [16] Y.-B. Ma, A. Grünebohm, K.-C. Meyer, K. Albe, and B.-X. Xu, Positive and negative electrocaloric effect in  $\text{BaTiO}_3$  in the presence of defect dipoles, *Phys. Rev. B* **94**, 094113 (2016).

- [17] Y.-B. Ma, B.-X. Xu, K. Albe, and A. Grünebohm, Tailoring the Electrocaloric Effect by Internal Bias Fields and Field Protocols, *Phys. Rev. Appl.* **10**, 024048 (2018).
- [18] X. Ren, Large electric-field-induced strain in ferroelectric crystals by point-defect-mediated reversible domain switching, *Nat. Mater.* **3**, 91 (2004).
- [19] P.-F. Zhou, B.-P. Zhang, L. Zhao, X.-K. Zhao, L.-F. Zhu, L.-Q. Cheng, and J.-F. Li, High piezoelectricity due to multiphase coexistence in low-temperature sintered (Ba,Ca)(Ti,Sn)O<sub>3</sub>–CuO<sub>x</sub> ceramics, *Appl. Phys. Lett.* **103**, 172904 (2013).
- [20] S. Murakami, T. Watanabe, T. Suzuki, T. Matsuda, and K. Miura, Effects of poling termination and aging process on piezoelectric properties of Mn-doped BaTi<sub>0.96</sub>Zr<sub>0.04</sub>O<sub>3</sub> ceramics, *Jpn. J. Appl. Phys.* **54**, 10ND05 (2015).
- [21] F. Li, M. J. Cabral, B. Xu, Z. Cheng, E. C. Dickey, J. M. LeBeau, J. Wang, J. Luo, *et al.*, Giant piezoelectricity of Sm-doped Pb(Mg<sub>1/3</sub>Nb<sub>2/3</sub>)O<sub>3</sub>-PbTiO<sub>3</sub> single crystals, *Science* **364**, 264 (2019).
- [22] F. Li, D. Lin, Z. Chen, Z. Cheng, J. Wang, C. Li, Z. Xu, Q. Huang, X. Liao, and L.-Q. Chen, Ultrahigh piezoelectricity in ferroelectric ceramics by design, *Nat. Mater.* **17**, 349 (2018).
- [23] M. Sanlialp, Z. Luo, V. V. Shvartsman, X. Wei, Y. Liu, B. Dkhil, and D. C. Lupascu, Direct measurement of electrocaloric effect in lead-free Ba(Sn<sub>x</sub>Ti<sub>1-x</sub>)O<sub>3</sub> ceramics, *Appl. Phys. Lett.* **111**, 173903 (2017).
- [24] M. Sanlialp, C. Molin, V. V. Shvartsman, S. Gebhardt, and D. C. Lupascu, Modified differential scanning calorimeter for direct electrocaloric measurements, *IEEE Trans. Ultrason. Ferroelectr. Freq. Control* **63**, 1690 (2016).
- [25] See Supplemental Material at <https://link.aps.org/supplemental/10.1103/PhysRevApplied.16.014033> for the information regarding the data used to construct the phase diagram, the structure analysis through X-ray diffraction, and ferroelectric and electrocaloric properties.
- [26] G. Arlt and H. Neumann, Internal bias in ferroelectric ceramics: Origin and time dependence, *Ferroelectrics* **87**, 109 (1988).
- [27] D. Damjanovic, in *The Science of Hysteresis*, edited by I. Mayergoyz, G. Betotti (Academic Press, New York, 2006), Vol. 3, Chap. 4, pp. 337.
- [28] R.-A. Eichel, P. Erhart, P. Träskelin, K. Albe, H. Kungl, and M. J. Hoffmann, Defect-Dipole Formation in Copper-Doped PbTiO<sub>3</sub> Ferroelectrics, *Phys. Rev. Lett.* **100**, 095504 (2008).
- [29] T. Wu, Y. Pu, T. Zong, and P. Gao, Microstructures and dielectric properties of Ba<sub>0.4</sub>Sr<sub>0.6</sub>TiO<sub>3</sub> ceramics with BaO-TiO<sub>2</sub>-SiO<sub>2</sub> glass-ceramics addition, *J. Alloys Compd.* **584**, 461 (2014).
- [30] F. Gao, X. Dong, C. Mao, W. Liu, H. Zhang, L. Yang, F. Cao, and G. Wang, Energy-storage properties of 0.89Bi<sub>0.5</sub>Na<sub>0.5</sub>TiO<sub>3</sub>-0.06BaTiO<sub>3</sub>-0.05K<sub>0.5</sub>Na<sub>0.5</sub>NbO<sub>3</sub> lead-free anti-ferroelectric ceramics, *J. Am. Ceram. Soc.* **94**, 4382 (2011).
- [31] Z. Yao, Z. Song, H. Hao, Z. Yu, M. Cao, S. Zhang, M. T. Lanagan, and H. Liu, Homogeneous/inhomogeneous-structured dielectrics and their energy-storage performances, *Adv. Mater.* **29**, 1601727 (2017).
- [32] M. Sanlialp, V. V. Shvartsman, M. Acosta, B. Dkhil, and D. C. Lupascu, Strong electrocaloric effect in lead-free 0.65Ba(Zr<sub>0.2</sub>Ti<sub>0.8</sub>)O<sub>3</sub>-0.35(Ba<sub>0.7</sub>Ca<sub>0.3</sub>)TiO<sub>3</sub> ceramics obtained by direct measurements, *Appl. Phys. Lett.* **106**, 062901 (2015).
- [33] X. Moya, E. Stern-Taulats, S. Crossley, D. González-Alonso, S. Kar-Narayan, A. Planes, L. Mañosa, and N. D. Mathur, Giant electrocaloric strength in single-crystal BaTiO<sub>3</sub>, *Adv. Mater.* **25**, 1360 (2013).
- [34] J. Li, Y. Bai, S. Qin, J. Fu, R. Zuo, and L. Qiao, Effects of long-and short-range ferroelectric order on the electrocaloric effect in relaxor ferroelectric ceramics, *Appl. Phys. Lett.* **109**, 162902 (2016).
- [35] Y. Liu, J. F. Scott, and B. Dkhil, Direct and indirect measurements on electrocaloric effect: Recent developments and perspectives, *Appl. Phys. Rev.* **3**, 031102 (2016).
- [36] Y.-B. Ma, N. Novak, J. Koruza, T. Yang, K. Albe, and B.-X. Xu, Enhanced electrocaloric cooling in ferroelectric single crystals by electric field reversal, *Phys. Rev. B* **94**, 100104 (2016).
- [37] K. Carl and K. H. Hardtl, Electrical after-effects in Pb(Ti,Zr)O<sub>3</sub> ceramics, *Ferroelectrics* **17**, 473 (1977).
- [38] X. Lou, Polarization fatigue in ferroelectric thin films and related materials, *J. Appl. Phys.* **105**, 024101 (2009).
- [39] A. Grünebohm, Yang-Bin Ma, M. Marathe, Bai-Xiang Xu, K. Albe, C. Kalcher, Kai-Christian Meyer, V. V. Shvartsman, D. C. Lupascu, and C. Ederer, Origins of the inverse electrocaloric effect, *Energy Technol.* **6**, 1491 (2018).
- [40] M. Otonicar and B. Dkhil, Electrocalorics hit the top, *Nat. Mater.* **19**, 9 (2020).
- [41] B. Nair, T. Usui, S. Crossley, S. Kurdi, G. G. Guzman-Verri, X. Moya, S. Hirose, and N. D. Mathur, Large electrocaloric effects in oxide multilayer capacitors over a wide temperature range, *Nature* **575**, 468 (2019).